Journal of Alloys and Compounds 509 (2011) 4002–4009

Contents lists available at ScienceDirect

Journal of Alloys and Compounds

journal homepage: www.elsevier.com/locate/jallcom

Influence of alcohol additives in the preparation of electrodeposited Pt–Ru catalysts on oxidized graphite cloths

Juan Manuel Sieben*[,1], Marta M.E. Duarte[2], Carlos E. Mayer

Instituto de Ingeniería Electroquímica y Corrosión, Universidad Nacional del Sur, B8000CPB Bahía Blanca, Argentina

ARTICLE INFO

Article history:
Received 20 September 2010
Received in revised form
29 December 2010
Accepted 3 January 2011
Available online 4 January 2011

Dedicated to our beloved friend Professor Carlos Enrique Mayer (in memoriam).

Keywords:
Electrodeposition
Pt–Ru alloys
Ethylene glycol
Ethanol
Methanol electro-oxidation

ABSTRACT

Carbon supported Pt–Ru catalysts were prepared by multiple cycles of potentiostatic pulses from aqueous diluted chloroplatinic acid and ruthenium chloride solutions in the presence of ethanol or ethylene glycol at pH 2 and 5. SEM images showed that the metallic deposit prepared at pH 2 consisted of large irregular agglomerates, whereas smaller globular particles were obtained at pH 5. In addition, the average particle size was considerably decreased in the presence of the stabilizers. The supported Pt–Ru alloys were tested as catalysts for methanol electro-oxidation in acid media. Electrocatalytic activity measurements indicated that the most active electrode was obtained with ethylene glycol as additive at pH 5.

1. Introduction

Direct methanol fuel cells (DMFCs) are attractive power sources for applications in low-emission electric vehicles, distributed home power generation and as power sources for small portable electronic devices due to their high energy density, simple set-up and the availability of liquid fuel [1]. Methanol is an attractive fuel due to its low cost, easy handling, storage and distribution, and because it can be obtained from biomass. However, there are several serious technological challenges that must be overcome before general application such as the slow kinetics of methanol oxidation reaction, the high cost of the catalysts [2], and the phenomenon of methanol crossover towards the cathode [3].

Nowadays, the main problem of DMFCs is the deficient activity and selectivity of anode electrocatalysts at a temperature compatible with available membranes. Platinum is the best catalyst for alcohol oxidation, but its surface is rapidly poisoned by strongly adsorbed CO-like intermediates produced in the dissociative adsorption of methanol molecules. Most research has been concentrated on the addition of some oxophilic metals as co-catalysts, forming bi-, tri- and multi-component alloys of Pt with elements such as Ru, Sn, W, Mo, Os, Ir, Pd, Co, Cu, Fe and Rh [4–10]. Amongst them, the Pt–Ru binary system has been found to exhibit excellent catalytic activity and high stability and is commonly used in state-of-the-art DMFCs.

Several studies have shown that the intrinsic activity of a supported Pt–Ru catalyst for methanol oxidation is determined by at least three factors: Ru concentration in the bimetallic catalyst, particle size and surface properties of the carbon support [11–12,4]. In addition, Gasteiger and Marković [13] have recently indicated that viable Pt-based catalysts (*i.e.* of high mass activities) must also have high turnover frequencies (number of electrons produced per active site per second under defined operating conditions) and a high degree of dispersion of the particles over the substrate. Therefore, it is very important to develop electrodes with a high surface area, good electrical conductivity and high stability in the fuel cell environment.

The production of Pt–Ru nanostructured catalysts by electrochemical techniques is advantageous in comparison with other techniques because it is a simple low cost operation which allows deposits of high purity and uniform deposition to be obtained. Besides, the metal particles can be deposited selectively at desired locations on the triple phase boundaries with enough electron, proton and reactant access, since the method requires both ionic and electronic access [14]. The catalyst structure, dispersion and parti-

* Corresponding author. Tel.: +54 291 4595182; fax: +54 291 4595182.
E-mail addresses: jmsieben@uns.edu.ar, jmsieben@yahoo.com (J.M. Sieben).
[1] Member of CONICET, Argentina.
[2] Member of Comisión de Investigaciones Científicas de la Provincia de Buenos Aires.

0925-8388/$ – see front matter © 2011 Elsevier B.V. All rights reserved.
doi:10.1016/j.jallcom.2011.01.003

cle size can be controlled by the adequate selection of overpotential (or current density). To achieve high dispersion of supported Pt–Ru nanoparticles, diverse electrochemical synthesis routes have been explored, such as galvanostatic step [15], potentiostatic step [16], galvanostatic pulse [17,18], potential pulse [19,20] and deposition followed by redox replacement [5,6,21]. For example, mesoporous Pt–Ru deposits supported on gold substrates with large electrochemical surface areas and high mass activities were prepared at constant potential by Franceschini et al. [16]. Coutanceau et al. [17] prepared highly dispersed nano-sized Pt–Ru deposits on Vulcan XC-72 by a galvanostatic pulse technique and reported a high catalytic activity for methanol oxidation. On the other hand, Sieben et al. [18] prepared Pt–Ru catalysts supported on oxidized graphite felt from solutions containing different complexants and found that the catalyst prepared using Na_2H_2EDTA as a stabilizer had high mass activity for methanol oxidation. Ando et al. [5] developed efficient Pt–Ru/C electrocatalysts for methanol oxidation with ultra low content of Pt and Ru using galvanic displacement of Pb by Pt and Ru.

Besides, the use of organic additives facilitates control of the crystallization process. Some organic compounds are frequently employed to avoid the agglomeration of nano-sized metal particles. For example, EDTA, tartaric acid and citric acid have been used as growth inhibitors in silver–zinc alloy [22], nickel–tungsten alloy [23], nickel [24] and platinum–ruthenium alloy electrodeposition [18]. Similar effects are observed in the chemical reduction of Pt and Pt–Ru in an aqueous solution containing one or more alcoholic components. For instance, ethylene glycol is able to act as a reducing agent at elevated temperatures and to prevent metal particles agglomeration [25,26].

This paper reports the preparation of carbon supported Pt–Ru catalysts by application of multiple cycles of potentiostatic pulses from diluted solutions of platinum and ruthenium salts containing ethanol (EtOH) and ethylene glycol (EG) as stabilizers. A study is made of the influence of pH and the presence of the stabilizers on the structural features, particle size, deposit dispersion and alloy composition and also of the electrochemical activities of these catalysts for methanol oxidation.

The size, dispersion and morphology of the nanoparticles are controlled via the solution pH and the stabilizer identity and concentration. It must be remarked that the preparation procedure is attractive because the stabilizers are simple organic compounds that can be eliminated by electrochemical oxidation without changing the properties of the bimetallic electrodes, while the stability of the solutions is preserved in the pH range between 2 and 5. Besides, all material electrodeposited on the substrate surface is expected to be available for the catalytic process.

2. Experimental

Graphite cloths (GC-10) of 1 cm^2 geometric area were used as catalyst support. Electrochemical measurements were carried out in a conventional glass cell at room temperature using a potentiostat PAR 273A. A platinum foil served as the counter-electrode, whereas a saturated calomel electrode (SCE) located in a Luggin capillary served as the reference electrode. An inert nitrogen atmosphere was maintained over the electrolyte. Electrochemical techniques such as linear and cyclic voltammetry and chronoamperometry were used to characterize the catalysts. The electrode activity for methanol oxidation was measured in 1 M CH_3OH + 0.5 M H_2SO_4 solution by cyclic voltammetry. Chronoamperometry curves were obtained at different potentials, applying potential pulses from an initial potential of 0 V.

The morphology of the catalyst surface and the particle size were analyzed using scanning electronic microscopy (SEM, EVO 40 LEO). The crystalline structure of the electrodes was characterized by X-ray diffraction (XRD) using a Rigaku Dmax III C diffractometer with a monochromated CuKα radiation source operated at 40 keV at a scan rate of 0.05° s^{-1}. Bulk composition analysis was performed using an energy dispersive spectroscopy (EDX) probe attached to a SEM microscope (JEOL 100). UV–vis spectrophotometer (Agilent 8453) was applied to evaluate the presence of the different Pt and Ru complex species formed. For UV–vis analysis all samples were diluted at a ratio of 1:50.

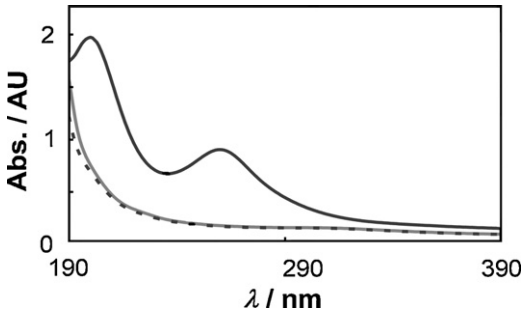

Fig. 1. UV–vis absorption spectra for freshly prepared solutions at pH 5 containing H_2PtCl_6 and $RuCl_3$, at room temperature. Without stabilizer (▬), EG (▬) and EtOH (▬ ▬).

Before the electrochemical deposition of the catalyst, the carbon supports were oxidized in 0.5 M H_2SO_4 to improve wettability, adsorption and cation exchange capacity [27]. The treatment consisted of an anodic potentiostatic polarization at 2 V for 300 s followed by a linear cathodic potential sweep down to −0.8 V (scan rate 1 mV s^{-1}).

The catalysts were prepared by electrodeposition using a diluted solution of 2 mM H_2PtCl_6 + 2 mM $RuCl_3$ in combination with *x* mM of ethylene glycol or ethanol (*x* = 20 or 200) as stabilizers. All solutions were prepared with bidistilled water and 0.5 M H_2SO_4 as supporting electrolyte. The pH of the solution was adjusted to 2 or 5 with 0.5 M NaOH solution. The following notation was used for the catalysts synthesized under the indicated conditions: (I) without stabilizer, (II) 20 mM EtOH, (III) 200 mM EtOH, (IV) 20 mM EG, and (V) 200 mM EG; while 'a' indicates pH 2 and 'b' indicates pH 5, *e.g.* Va.

Electrodeposition was carried out using 30 successive cycles of potentiostatic pulses (see Supplementary Fig. S1). The sequence of alternate negative and positive potentiostatic pulses was selected to achieve the formation and growth of crystallites during the cathodic pulse, and the oxidation of hydrogen, EG or EtOH throughout the anodic pulse. After deposition, the electrodes were thoroughly rinsed with bidistilled water and tested in sulfuric acid solution. A lineal potential sweep from −0.25 to 0.5 V was applied at a rate of 50 mV s^{-1}.

The active surface area of the electrocatalysts was determined by copper underpotential deposition (Cu-UPD) [28]. First reference voltammograms were obtained in 0.1 M H_2SO_4 cycling between −0.25 V and 0.8 V at a scan rate of 10 mV s^{-1}. The electrodes were polarized at 0 V for 300 s to reduce RuO_x formed during the cyclic voltammetry. The Cu-UPD experiments were carried out in 0.1 M H_2SO_4 and 2 mM $CuSO_4$ solution. The working electrodes were polarized at 0.059 V for 300 s to form a monolayer of copper on the catalyst surface. A linear voltammetric scan with a scan rate of 10 mV s^{-1} was then performed between 0.059 V and 0.8 V to remove the adsorbed copper monolayer (see Supplementary Fig. S2). The charges obtained for the copper stripping were corrected for the charges associated with background processes and oxide growth by subtracting the charge obtained from the reference scan in the same potential range. The integration of the peak area corresponding to the Cu-UPD stripping was used to determine the electroactive surface area, assuming an adsorption ratio of a single Cu atom to each surface metal atom and a monolayer charge of 420 μC cm^{-2} [29]. Current densities for methanol electro-oxidation are referred to the active surface area determined by Cu-UPD.

The loading of the prepared catalysts was estimated in selected samples using ICP-AES (Shimadzu 1000 model III). The quantity of either metal deposited under different conditions was found to be between 0.22 and 0.33 mg cm^{-2}.

3. Results and discussion

3.1. UV spectrophotometric analysis of platinum and ruthenium solutions

Fig. 1 shows the UV spectral change when the different stabilizing agents were added. In the case of H_2PtCl_6 + $RuCl_3$ solution without stabilizer, there are two absorbance peaks at ~200 and ~260 nm. The peak at 260 nm is the result of the ligand-to-metal charge transfer transition in the $PtCl_6^{2-}$ ions [30], whereas the first peak may be attributed to the partial hydrolysis reaction of $PtCl_6^{-2}$ to form chloroaqua or hydroxy complexes by the following sequence of reactions (see Ref. [31] and references therein):

$$PtCl_6^{2-} + H_2O \rightleftarrows PtCl_5(H_2O)^- + Cl^- \quad (1)$$

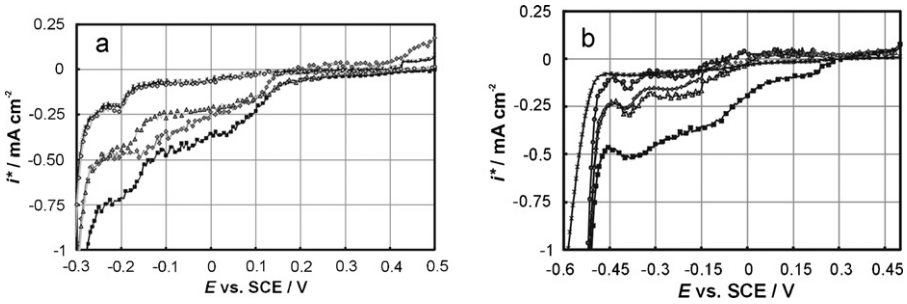

Fig. 2. Voltammetric curves for a GC-10 support in 2 mM H_2PtCl_6 + 2 mM $RuCl_3$ at (a) pH 2 and (b) pH 5. Without stabilizer (-■-), 20 mM EG (-♦-), 200 mM EG (-*-), 20 mM EtOH (-▲-), and 200 mM EtOH (-●-). Sweep rate 0.5 mV s^{-1}.

$$PtCl_5(H_2O)^- + H_2O \rightleftarrows PtCl_4(H_2O)_2 + Cl^- \quad (2)$$

$$PtCl_6^{2-} + OH^- \rightleftarrows PtCl_5(OH)^{2-} + Cl^- \quad (3)$$

Moreover, the characteristic ruthenium chloride complex absorption at 210 nm [32] is masked by the H_2PtCl_6 absorption at this wavelength due to the lower absorbance signal of the ruthenium aqueous species.

The two characteristic absorbance bands disappear upon the addition of EG and EtOH stabilizing agents. This behavior can be associated with the promoted dechlorination of Pt and Ru precursor salts [33], *i.e.* the –OH functionalities in EG and EtOH molecules replace the chloro ligands in order to form more stable complexes [34].

3.2. Voltammetric measurements for the codeposition of Pt and Ru at different pH

Fig. 2 shows the linear sweep voltammetry curves corresponding to graphite cloth (GC-10) electrodes in aqueous solutions containing H_2PtCl_6 and $RuCl_3$ at different pH with and without the stabilizing agents. The cathodic limit was selected at −0.3 V and −0.6 V for the experiments at pH 2 and 5, respectively. These potentials were slightly more negative than the onset of H_2 evolution on Pt–Ru particles. Pt electrodeposition, according to previous studies [35], is controlled by mass transport of species in solution. The curve corresponding to Pt and Ru deposition without stabilizer at pH 2 (Fig. 2(a)) shows that Pt deposition starts at about 0.35 V. Moreover, three overlapping reduction waves can be seen with half wave potentials at 0.08 V, −0.05 V and −0.2 V, where the last wave is probably coupled with the discharge of H^+ ions on Pt nuclei. The three reduction waves can be explained by slow nucleation of Pt centers and the reduction of Pt(+IV) to Pt metal from solutions that contain substantial amounts of $PtCl_6^{2-}$ and two species resulting from the hydrolysis reaction (Eqs. (1) and (2)) [36]. Reduction of each complex is to be expected, and the multiple cathodic waves would be observed if each complex underwent the reaction:

$$Pt(IV) + 4e^- \rightarrow Pt \quad (4)$$

although the presence of Pt(+II) as a stable intermediate [27] cannot be entirely discarded from this analysis.

It is known that Ru can be codeposited with Pt on carbon at a lower overpotential than when it is deposited as a single metal, favored kinetically by the platinum nuclei formed over the carbon support [26]. Besides, facilitation of $RuCl_5(H_2O)^{2-}$ discharge under conditions of parallel discharge of $PtCl_6^{2-}$ and $PtCl_4^{2-}$ can be considered as another possible kinetic reason [37]. In accordance with the literature data [37], ruthenium codeposition seems to be possible in the region where no evidence of Ru deposition on carbon is found, *i.e.* Ru(+III) codeposition may begin in the potential zone where $PtCl_5(H_2O)^-$ specie is reduced (−0.15 to 0 V).

When the stabilizers are added to the solution, a shift towards more negative potentials in Pt(+IV) reduction process is observed. The electrodeposition of Pt begins at 0.2 V in the solution containing 20 mM of EtOH or EG, whereas Pt(+IV) reduction starts at ∼0.15 V when the concentration of the stabilizers is increased 10 times (200 mM). At low concentration of the alcohols, three reduction waves are visible, although the second wave is more drawn out along the axis and the first wave becomes shorter. However, only two reduction waves are visible when 200 mM of EtOH or EG are added or at least the first two waves become indiscernible. Experiments at pH 5 lead to voltammetric curves with a few differences as regards those obtained at pH 2. For example, the beginning of the reduction process is shifted to more negative potentials and the peak associated with the discharge of H^+ ions on Pt nuclei becomes more clearly defined although appearing at potentials more negative than at pH 2.

The voltammetric behavior observed with the stabilizers at both pHs may be associated with several causes: (i) the capability of the stabilizing agent to form complexes with the metal ions, (ii) the irreversible adsorption of organic molecules which inhibits particle growth and (iii) the reduction in the polarity of the electrolyte which improves ion exchange of Pt and Ru ions with the support surface oxide groups. The first point, as was suggested previously, can be associated with the substitution of the chloro ligands by the –OH functionalities in EG and EtOH molecules in order to form more stable complexes [34]. The addition of EG and EtOH with relative permitivities of 37.8 and 24 respectively, may influence the simultaneous electrodeposition of Pt and Ru when the alcohol concentration is high. The addition of alcohols may lead to a decreased ionic strength in the deposition bath, augmenting the interparticle electrostatic repulsion and thus influencing the nucleation-growth mechanism [38].

3.3. Physicochemical analysis of the working Pt–Ru catalysts

The atomic composition of Pt–Ru catalysts was determined by the EDX technique. The results are listed in Table 1. The Ru content in the different samples is in the expected order, taking into account the procedure used to deposit the metals. Pt enrichment of electrodeposits as compared with Pt:Ru ratio in the solution has been observed by several authors for a broad range of deposition parameters [29,37,39]. Gavrilov et al. [37] suggested that this behavior was due to kinetic, not thermodynamic hindrances.

The ruthenium content of the catalysts prepared with the stabilizers at pH 2 is slightly lower than that on the catalyst prepared without a stabilizer, whereas the inverse dependence is observed at pH 5. This behavior could be a consequence of the interplay between the pH of the deposition bath and the presence of the stabilizers, since both factors influence the rate of Ru electrodeposition.

Table 1
Synthesis conditions and physical parameters of supported Pt–Ru catalysts.

Electrode	Solution pH	Stabilizer	Stabilizer concentration (mM)	$X_{Ru(EDX)}$	a_{fcc} (nm)	$X_{Ru(XRD)}$[a]	d_p (nm)[b]	d_c (nm)[c]	S (cm^2)[d]	S_w (m^2 g^{-1})
Ia	2	–	–	0.15	0.3902	0.17	200–300	18	16.8	–
IIa	2	EtOH	20	0.14	0.3904	0.15	100–300	7	46.5	–
IIIa	2	EtOH	200	0.13	0.3905	0.15	100–200	5	78.1	23.7
IVa	2	EG	20	0.13	0.3907	0.13	200–300	8	28.2	–
Va	2	EG	200	0.13	0.3908	0.12	100–200	6	55.3	–
Ib	5	–	–	0.12	0.3907	0.13	100–150	12	40.2	12.1
IIb	5	EtOH	20	0.14	0.3907	0.13	75–100	7	55.4	–
IIIb	5	EtOH	200	0.15	0.3907	0.13	50–75	5	78.2	33.9
IVb	5	EtOH	20	0.13	0.3908	0.12	20–60	5	86.7	–
Vb	5	EtOH	200	0.15	0.3905	0.15	20–40	4	95.8	42.8

X_{Ru}, alloyed Ru atomic fraction; a_{fcc}, lattice parameter; d_p, particle size; d_c, crystallite size; S, active surface area; S_w, specific surface area.
[a] Estimated from lattice parameter using the Vegard's law (Eq. (5)).
[b] Determined from SEM analysis.
[c] Determined from Debye–Scherrer equation.
[d] Determined from Cu-UPD measurements.

Fig. 4 shows that the simultaneous hydrogen evolution begins at about −0.4 V at pH 5, whereas it starts at −0.2 V at pH 2. It seems probable that adsorbed hydrogen will compete with ruthenium adatoms for the free platinum sites during the first stages of Pt–Ru electrodeposition producing accumulation or deficit of Ru atoms on the bimetallic agglomerate surface.

Seminal reports of some authors [40,41] disclosed that the shape of the voltammograms for bimetallic Pt–Ru catalysts was very susceptible to changes in their surface composition. Gasteiger et al. [40] reported major changes in the voltammetric response of well characterized sputter-cleaned single-phase Pt–Ru alloys containing from 7 to 100% surface Ru content. They observed that the enrichment of the surface with Ru causes the increase of the pseudo-capacitive current in the double layer zone and the progressive loss of the distinctive feature of pure Pt in the "hydrogen region". On the other hand, Frelink et al. [41] found a good correlation between the potential of the surface oxide reduction peak on the CVs and the surface catalyst composition upon Ru electrodeposition on the Pt surface.

Fig. 3 shows that the stabilizers have some influence on the shape of CVs of Pt–Ru supported catalysts in sulfuric acid solution. The increment of the synthesis solution pH results in an attenuated intensity of the characteristic hydrogen adsorption/desorption peaks and a reduction of the coulombic charge (*e.g.* the cathodic charge is reduced at about 30% for catalyst III) in the so called "H-UPD zone". Nevertheless, the pseudo-capacitive current in the double layer region stays almost unchanged. An attempt to obtain some values for the surface composition was made using the method described by Gasteiger et al. [40]. However, the current contribution of the oxygenated surface groups from the carbon substrate to the pseudo-capacitive behavior of the double layer makes it impossible to gain reliable information. The aforementioned reduction of the hydrogen desorption charge observed for the catalysts prepared at pH 5 can nevertheless be considered as an indication of the surface enrichment in ruthenium of the catalysts prepared under these conditions.

XRD patterns of the catalysts are shown in Fig. 4. The diffractograms show three peaks characteristic of Pt face centered cubic (*fcc*) crystalline structure at approximately 2θ values of 40.2°, 46.1° and 68.2°, which are associated with the [1 1 1], [2 0 0] and [2 2 0] planes. Comparing with the reflections of pure Pt the diffraction peaks for Pt–Ru/GC-10 are shifted slightly to higher 2θ values. The slight shift of the diffraction peaks reveals the formation of an alloy (*i.e.* solid solution) involving the incorporation of Ru atoms into the *fcc* structure of Pt. It is important to note that no diffraction peaks indicate the presence of either pure Ru or Ru-rich hexagonal close packed (*hcp*) phase, but their presence cannot be discarded because metallic ruthenium or amorphous ruthenium oxides may be present in very small amounts over the surface of the bimetallic particles.

The peak profiles in XRD patterns were obtained by integration of the respective areas after peak deconvolution using the Marquardt algorithm. A lattice constant of 0.3922 ± 0.0004 nm was determined for Pt/GC-10 in good agreement with 0.3923 for pure Pt, whereas values between 0.3902 and 0.3908 ± 0.0005 nm were obtained for Pt–Ru/GC-10 catalysts prepared with and without the stabilizers (Table 1). In accordance with the Vegard's law (Eq. (5)), the nominal Ru content of Pt–Ru catalysts estimated from XRD patterns agrees with that measured from EDX analysis.

$$a_{Pt} = a_{Pt-Ru} - 0.0124X_{Ru} \quad (5)$$

where a_{Pt} and a_{Pt-Ru} (nm) are the lattice parameters of Pt/GC-10 and Pt–Ru catalysts respectively, and X_{Ru} is the alloyed Ru atomic fraction.

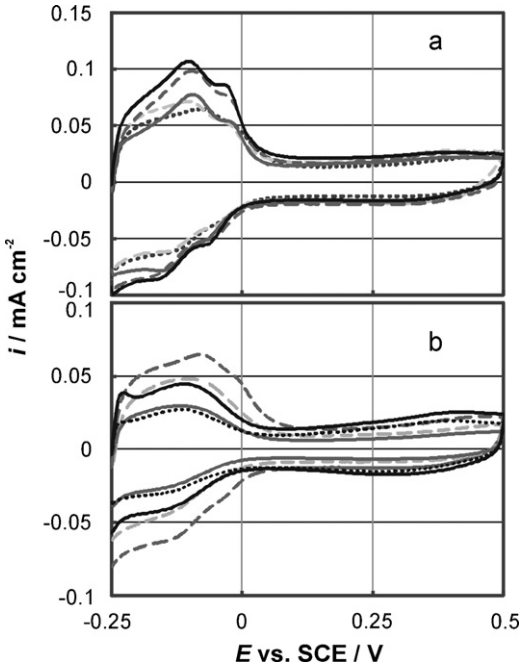

Fig. 3. Cyclic voltammograms for carbon supported Pt–Ru catalysts in 0.5 M H_2SO_4 at a scan rate of 50 mV s^{-1}. Catalysts prepared at (a) pH 2 and (b) pH 5. Without stabilizer (••••), 20 mM EG (• • •), 200 mM EG (— — —), 20 mM EtOH (——), and 200 mM EtOH (——).

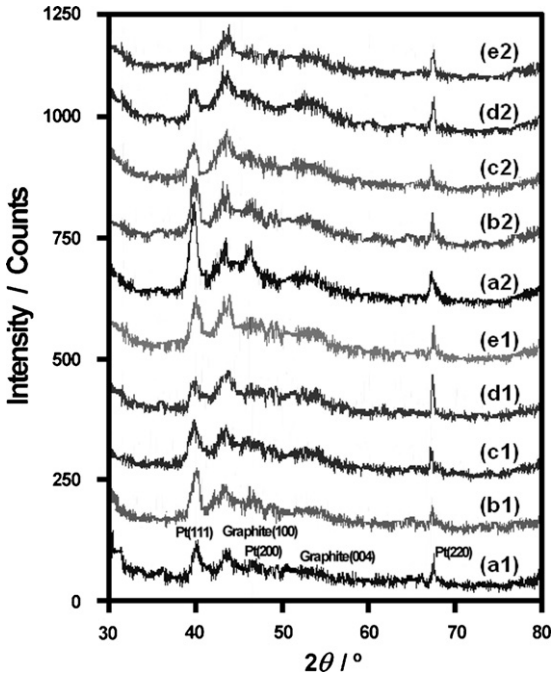

Fig. 4. XRD spectra of Pt–Ru/GC-10 catalysts prepared by successive cycles of potentiostatic pulses: pH 2, without stabilizer (a1), 20 mM EtOH (b1), 200 mM EtOH (c1), 20 mM EG (d1) and 200 mM EG (e1); pH 5,without stabilizer (a2), 20 mM EtOH (b2), 200 mM EtOH (c2), 20 mM EG (d2) and 200 mM EG (e2).

Debye–Scherrer's equation was used to estimate the average Pt–Ru crystallite size from the most distinct peak, Pt [1 1 1] centered around $2\theta = 40.2^{\circ}$. The size of the crystallites (more properly, the coherence length of crystalline domains) measured from diffractograms are listed in Table 1. It can be seen that the addition of the stabilizers at both pHs decreases the diameter of the crystallites, in agreement with results reported by several authors [25,26,33].

SEM micrographies of Pt–Ru catalysts on oxidized graphite cloths are shown in Fig. 5. At pH 2 the GC-10 substrate is completely covered with metal particles, grouped in large irregular agglomerates distributed over the support surface (Fig. 5(a1)–(c1)). The irregular shape of the islands can be associated with a deposition process occurring at mass-transfer or mixed control regime [34,35]. Furthermore, the irregular morphology may be related to the interplay between primary and secondary nucleation resulting in the formation of complex micro and nanograined Pt structures [34]. Besides, simultaneous hydrogen evolution on the surface of the metal nuclei formed at the first stages of the deposition process can contribute to the morphology observed for the catalysts synthesized at pH 2. The mean particle size (more precisely, agglomerate size) of Pt–Ru/GC-10 catalysts is listed in Table 1. The catalyst IIIa exhibits the lowest particle size followed by catalyst Va, indicating that EtOH acts as a better stabilizer than EG at pH 2.

On the other hand, a higher average size and a high degree of coalescence are observed in catalyst Ia. Gloaguen et al. [44] disclosed that Pt particles gradually grow during the electrodeposition procedure and eventually overlap producing the coalescence of individual particles. Zoval et al. [45] concluded that Pt electrodeposition on HOPG takes place via formation of particles 10–20 nm in diameter followed by their lateral sticking through surface diffusion, which results in particle agglomeration. In fact, both processes can contribute to the Pt–Ru catalyst morphology observed in SEM images.

At pH 5 the bimetallic particles exhibit a uniform size and a globular shape, appearing regularly distributed over the support surface with lower average size and higher dispersion than those obtained at lower pH (Fig. 5(a2)–(c2)), which is in agreement with results obtained by other authors [26,46]. As was suggested by Bock et al. [26], the synthesis solution pH is a key factor that influences the noble metal dispersion and the particle size. The morphological characteristics of the deposits in the case of the catalysts IIIb and Vb can be associated with the chelating capability of carboxylate anions and the irreversible adsorption of organic molecules, which restrict particle growth and prevent particle agglomeration.

The coexistence of Pt and hydroxylated species ($PtOH_{ads}$ and $RuOH_{ads}$) formed during the anodic pulses on the freshly electrodeposited nanoparticles is probably responsible for the catalytic oxidation of EtOH and EG, which would lead to the formation of CH_3COOH and $C_2O_4H_2$ (or $HOCH_2COOH$) respectively [39,40], through the so-called bifunctional mechanism [39]. The carboxylate anions of these molecules (acetate, glycolate and oxalate) can interact with the noble metal ions forming chelate-type complexes. At pH 5 the amount of free carboxylate is expected to be high, so the stabilizing action of the anion should be important as was observed for complexants such as citrate and EDTA [18]. Nevertheless, this effect should not be so important at pH 2 because free carboxylate anion groups would be almost non-existent and the carboxyl group is believed to act as a poor stabilizer [26,46].

Besides, the surface diffusion of metal adatoms can be hindered by the dissociative adsorption of EtOH or EG during the anodic pulses, essentially by forming strongly adsorbed by-products on the catalyst surface [47,48], that is, the free electron pairs in the oxygen atoms would interact strongly with Pt–Ru particles and therefore the inhibiting effect would be very strong as it is observed for other systems [49].

However, the characteristics of the deposit shown in Fig. 5(a2) appear to be anomalous if it is considered that no stabilizer was used to prepare the catalyst. In other words, no changes in the morphology should be expected. However, more OH^- ions are available at pH 5, and more Cl^- in $[PtCl_6]^{2-}$ complex ions can be replaced by OH^- through the hydrolysis reaction (Eq. (3)) [31] (similar behavior is expected for Ru chloride species), thus decreasing the deposition rate of Pt and Ru complex ions.

Amongst the catalysts prepared at pH 5, catalyst Vb exhibits the lowest mean particle size followed by catalyst IVb and catalyst IIIb. This behavior can be related to the better stabilization obtained with EG addition, especially due to the presence of glycolate and oxalate anions resulting from the EG oxidation reaction [26].

Table 1 shows the parameters habitually used to characterize the supported Pt–Ru catalysts. It can be seen that the active surface area, S, and the specific surface area, S_w, are significantly affected by the presence of EtOH and EG in the solution. In general, the catalysts prepared at low pH exhibit S values lower than those catalysts prepared at high pH. At pH 2 the electrodes prepared by adding elevated EtOH concentration (IIIa) exhibit the highest active surface area, followed by that prepared adding high EG concentration (Va); whereas at pH 5 the inverse behavior is observed (S of Vb > IIIb). This result can be related to the decrease in Pt–Ru particle size and a remarkably high dispersion of alloy particles. Moreover, it can be seen that S_w increases almost three times when the catalysts are prepared using EG and EtOH. On the other hand, it can be observed from the results that the catalyst loading decreases when the pH of the solution is increased. This observation agrees well with results reported by Kim et al. [46] for Pt/C catalysts prepared by the polyol technique at different pHs. The authors concluded that the reduction of Pt loading by increasing the pH of the solution is caused mainly by the electrostatic repulsive force between carbons and Pt particles. However, in this case the diminution of catalyst loading by increasing pH is probably related to the slower reduction rate of Pt and Ru species resulting from the hydrolysis reaction (Eq. (3)). Besides, in the presence of stabilizers, as the solution becomes less acidic, more stable complex species are formed, with stronger

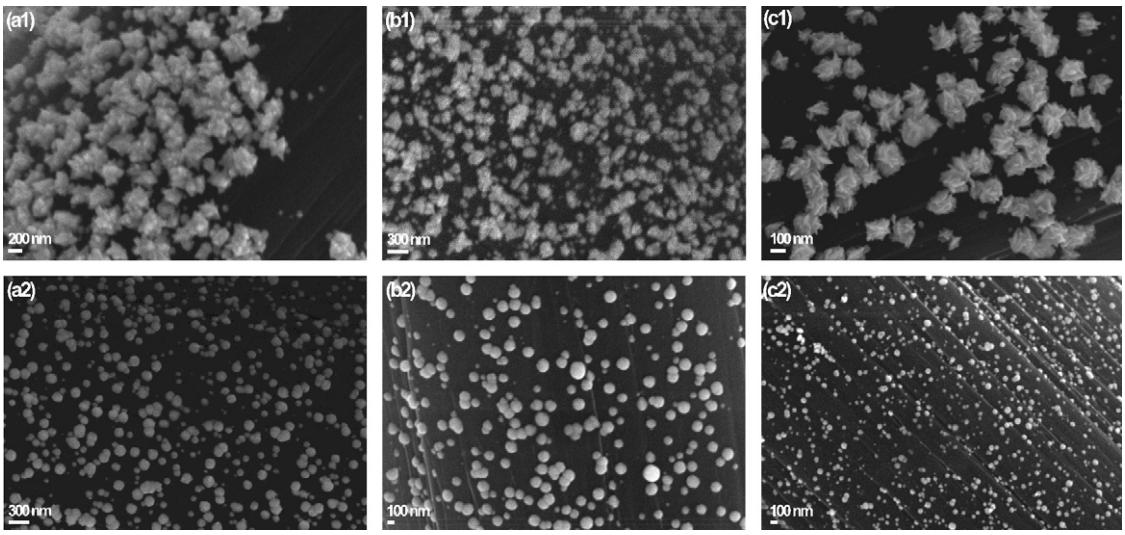

Fig. 5. Top-view SEM images of Pt–Ru/GC-10 electrodes comparing the particles obtained using different stabilizing agents. pH 2, without stabilizer (a1), EtOH (b1) and EG (c1); pH 5 without stabilizer (a2), EtOH (b2) and EG (c2). Pt–Ru/GC-10 catalysts prepared by successive cycles of potentiostatic pulses.

Table 2
Catalytic activities of supported Pt–Ru/GC-10 catalysts.

Electrode	i_{pf} (mA cm^{-2})[a]	i (mA cm^{-2})[b]	i (A g^{-1})[b]
Ia	0.57	0.16	–
IIa	1.00	0.28	–
IIIa	2.59	0.63	149.3
IVa	0.91	0.24	–
Va	1.49	0.42	–
Ib	1.03	0.31	37.5
IIb	1.84	0.45	–
IIIb	3.05	0.93	315.3
IVb	2.05	0.62	–
Vb	4.89	1.44	614.9

[a] Data from cyclic voltammetry experiments, tenth cycle.
[b] Data from quasi-stationary measurements at 0.4 V.

metal–ligand bonds, and hence, Pt and Ru species are less prone to be reduced [26].

To summarize the increase in the pH of the solution and the addition of the stabilizers is helpful in controlling the size and morphology of metallic particles and in improving catalyst dispersion with a reduction in the metal loading.

3.4. Methanol electro-oxidation

Figs. 6 and 7 show the cyclic voltammograms recorded at 50 mV s^{-1} and current transient measurements carried out at 0.4 V for 300 s, respectively in 1 M CH_3OH + 0.5 M H_2SO_4 solution at room temperature for catalysts prepared at pH 2 (a) and pH 5 (b). The results of methanol electro-oxidation for the electrodes prepared under the different conditions are summarized in Table 2.

In general, for all the electrodes the onset of methanol oxidation reaction takes place at potentials below 0.2 V, which is associated with the formation of OH_{ads} species on Ru atoms at potentials more negative than on Pt atoms, through the so-called bifunctional mechanism [39,50]. A methanol oxidation peak appears during the forward scan at about 0.65 V and another anodic peak can be seen on the reverse scan at lower potentials, due to the removal of incompletely oxidized species formed in the forward scan.

The catalysts prepared at pH 5 exhibit better performances than those prepared at pH 2. The voltammograms of the catalysts synthesized at pH 2 show that PtRu/GC-10 catalyst IIIa has higher activity for methanol oxidation, followed by electrode Va. On the other hand, catalyst Vb becomes the most active of the catalysts prepared at pH 5, followed by catalyst IIIb.

The quasi-stationary experiments showed the same tendency as that observed on the CVs. Current transients are characterized by a rapid current decay at short time, followed by a quasi-steady-state current at times longer than 120 s. This current decay is observed in the literature for Pt–Ru catalysts at different temperatures and methanol concentrations [39,51]. The main cause of the current decay is the blocking of the active sites by the poisoning species. In this way, carbon monoxide specie acts as poison but possibly it is not the only one because the reaction is deactivated even at the potentials where CO is oxidized by the presence of OH species adsorbed on Ru atoms.

A comparison of the dependence of i upon S, d_p and the catalyst loading for the electrodes prepared under different deposition conditions indicate that better performances for methanol oxidation are obtained using the electrodes that have lower agglomerate size and higher dispersion of the bimetallic particles over the carbon substrate (higher active surface area), which is in accordance with data in the literature [52,53]. Catalysts prepared at low pH, even those synthesized adding stabilizers, exhibit a high degree of particle agglomeration, so that part of the catalyst surface will be less accessible to the alcohol solution.

Furthermore, the superior activity of the electrodes prepared at pH 5 may be associated with the slightly higher concentration and uniform dispersion of Ru atoms on the catalyst surface.

However, these features are not enough to justify the difference greater than a factor of two between the specific activities for samples Vb and IIIa, and the reason why the activity for methanol electro-oxidation increases with both the active surface area and the specific surface area. Another explanation would be that mass transport limitations rather than intrinsic electrocatalytic effects are responsible for such behavior (Seidel et al. [54] and references therein). The presence of transport problems due to the characteristics of the catalyst materials (substrate properties, particle size and morphology, catalyst dispersion, and metal loading) could explain the unusual behavior observed in this case.

On the other hand, the tridimensional structure of the carbon support can contribute to the mass transport issue since methanol must diffuse through the material fiber arrangement to reach the inner Pt–Ru particles. Therefore, if most methanol molecules are

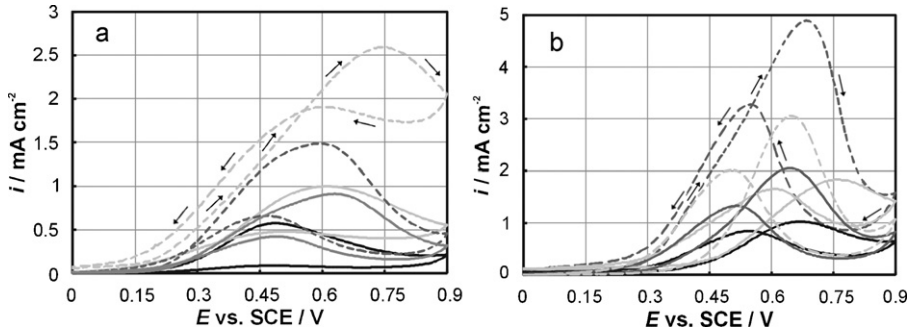

Fig. 6. Cyclic voltammograms (tenth cycle) for Pt–Ru/GC-10 electrodes in 1 M CH_3OH/0.5 M H_2SO_4, at room temperature. pH 2 (a) and Ph 5 (b). Without stabilizer (▬), 20 mM EtOH (▬), 200 mM EtOH (▬), 20 mM EG (▬) and 200 mM EG (▬). Scan rate 50 mV s^{-1}.

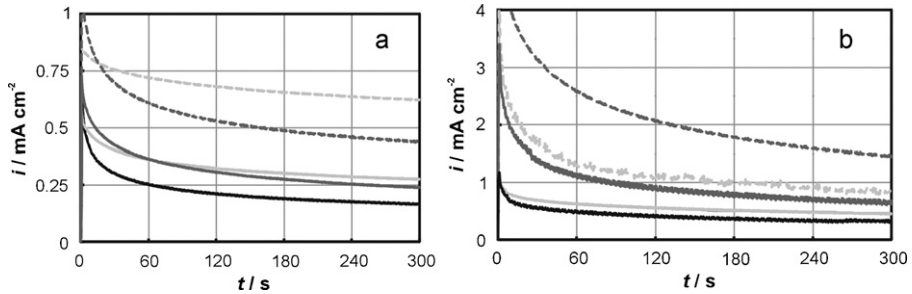

Fig. 7. Chronoamperometry curves at 0.4 V vs. SCE for Pt–Ru/GC-10 electrodes in 1 M CH_3OH/0.5 M H_2SO_4, at room temperature from an initial potential of 0 V vs. SCE. pH 2 (a) and pH 5 (b). Without stabilizer (▬), 20 mM EtOH (▬), 200 mM EtOH (▬), 20 mM EG (▬) and 200 mM EG (▬).

consumed at the electrode surface only a few will arrive at the inner catalyst particles [35]. This behavior may be more pronounced in the catalyst that exhibits large agglomerates and poor dispersion on the external cloth surface.

A comparison of electrocatalytic activities for Pt–Ru supported electrodes published by different research groups is difficult to achieve due to the diverse testing conditions (alcohol concentration, temperature and set-up for performing electrochemical experiments) and catalyst materials (synthesis methods, catalyst characteristics and material support properties). Despite these problems, mass activity with respect to time from chronoamperometric data obtained after 300 s and methanol oxidation current peak on the CV of the most active home-made Pt–Ru/GC-10 catalyst (Vb) can be compared with some chemically-synthesized catalysts reported in the literature [55–59]. Higher catalytic activity is obtained with catalysts Vb despite the higher particle size of the electrodeposit (20–40 nm against 2–8 nm), the lower platinum loading and some degree of agglomeration. For example, Zhao et al. [55], Kim et al. [56], Chetty et al. [57] and Jiang et al. [58] reported peak current densities between 200 and 340 A g^{-1} (or between 0.46 and 0.73 mA cm^{-2}) for $Pt_{0.5}Ru_{0.5}$ catalysts dispersed on different carbon supports, with average particle sizes in the range of 2–8 nm, specific surface areas in the range of 44–57 m^2 g^{-1} and Pt loadings between 0.3 and 2 mg cm^{-2}, while Li and Hsing [59] reported that a $Pt_{0.51}Ru_{0.49}$/C catalyst with 0.2 mg cm^{-2} Pt loading, an average particle size of *ca.* 2.5 nm, and a S_w value of about 41 m^2 g^{-1} showed a peak current density of about 400 A g^{-1} (0.56 mA cm^{-2}).

The enhanced performance of electrode Vb can be mainly explained by the better Pt–Ru particle utilization, while in the chemical synthesized catalysts, part of the catalytic material is inactive for the oxidation reaction.

Besides, some aspects of this behavior may also be associated with the nanostructured nature of the electrodeposits; that is the multi-grained structures of the catalysts (nano-sized grains interconnected via grain boundaries) may act similarly to low coordinated sites (steps and kinks) on single crystalline and other extended surfaces, which will enhance the adsorption of the alcohols and promote CO oxidation [60 and references cited therein].

Moreover, some differences in the catalytic performance of the electrodes can be attributed to changes in the alloy composition. In general, surface reactions require a specific crystal orientation and a suitable atomic configuration at the surface favoring an appropriate bonding situation of the reactants, as was recently outlined by Hoster et al. [61].

Finally, the interaction of metal clusters with support sites having specific properties such as acidity or basicity could decrease the adsorption strength of methanolic residues and the oxidized groups would facilitate the accessibility of methanol to the electroactive surface [62].

Although studies under more real fuel cell conditions need to be carried out for these electrode materials, the results of this preliminary work shows that the catalysts prepared in this work exhibit better methanol electro-oxidation activities than some catalysts prepared by chemical methods. Further studies are in course mainly focused on the evaluation of the stability and performance of the Nafion® covered Pt–Ru catalysts in long-term experiments and the use of these electrodes in the fabrication of membrane electrode assemblies (MEAs) to test the catalysts under real DMFC operating conditions. Besides, the synthesis procedure will need to be further optimized to reduce particle size and to enhance particle dispersion.

4. Conclusions

Nanostructured Pt–Ru catalysts supported on an oxidized graphite cloth were successfully prepared by a simple electrochemical technique in ethanol or ethylene glycol aqueous solutions at pH 2 and 5. Solid solutions of low Ru content (between 12 and 17%) were formed. The catalyst composition was only slightly affected by the solution pH and the presence of the alcohols.

The addition of the stabilizers EtOH and EG, along with the solution pH, were critical to determine the size, shape and dispersion of the particles of the resulting Pt–Ru catalysts.

Electrodes with better properties were obtained with higher concentrations of EtOH and EG at pH 5. These materials exhibited a better performance for methanol oxidation than those prepared at pH 2. This result can be related to a remarkable improvement of the deposit dispersion, a reduction of particle size and a higher active surface area of the catalyst. Furthermore, mass transport limitations are suggested to explain some unusual behavior of the electrodeposited catalysts.

Acknowledgements

The authors thank the CIC and SECyT UNS, Argentina, for financial support. The assistance by Dr. Graciela Mas in the XRD measurements is also acknowledged.

Appendix A. Supplementary data

Supplementary data associated with this article can be found, in the online version, at 10.1016/j.jallcom.2011.01.003.

References

[1] A.M. Zainoodin, S.K. Kamarudin, W.R.W. Daud, Int. J. Hydrogen Energy 35 (2010) 4606–4621.
[2] M.P. Hogarth, T.R. Ralph, Platinum Metals Rev. 46 (2002) 146–164.
[3] H. Hoster, T. Iwasita, H. Baumgartner, W. Vielstich, J. Electrochem. Soc. 148 (2001) A496–A501.
[4] Y.J. Song, S.B. Han, J.M. Lee, K.W. Park, J. Alloys Compd. 473 (2009) 516–520.
[5] Y. Ando, K. Sasaki, R. Adzic, Electrochem. Commun. 11 (2009) 1135–1138.
[6] S.H. Ahn, O.J. Kwon, S.-K. Kim, I. Choi, J.J. Kim, Int. J. Hydrogen Energy 35 (2010) 13309–13316.
[7] Z.B. Wang, P.J. Zuo, G.P. Yin, J. Alloys Compd. 479 (2009) 395–400.
[8] I. Ávila-García, C. Ramírez, J.M. Hallen López, E.M. Arce Estrada, J. Alloys Compd. 495 (2010) 462–465.
[9] Y.M. Alyousef, M.K. Datta, K. Kadakia, S.C. Yao, P.N. Kumta, J. Alloys Compd. 506 (2010) 698–770.
[10] C.F. Tsai, K.-Y. Yeh, P.W. Wu, Y.F. Hsieh, P. Lin, J. Alloys Compd. 478 (2009) 868–871.
[11] C.T. Hsieh, Y.W. Chou, W.Y. Chen, J. Alloys Compd. 466 (2008) 233–240.
[12] Y. Liang, J. Li, Q.C. Xua, R.Z. Hu, J.D. Lin, D.W. Liao, J. Alloys Compd. 465 (2008) 296–304.
[13] H.A. Gasteiger, N.M. Marković, Science 324 (2009) 48–49.
[14] C.R.K. Rao, D.C. Trivedi, Coord. Chem. Rev. 249 (2005) 613–631.
[15] A. Bauer, E.L. Gyenge, C.W. Oloman, Electrochim. Acta 51 (2006) 5356–5364.
[16] E.A. Franceschini, G.A. Planes, F.J. Williams, G.J.A.A. Soler-Illia, H.R. Corti, J. Power Sources 196 (2011) 1723–1729.
[17] C. Coutanceau, S. Brimaud, C. Lamy, J.-M. Léger, L. Dubau, S. Rousseau, F. Vigier, Electrochim. Acta 53 (2008) 6865–6880.
[18] J.M. Sieben, M.M.E. Duarte, C.E. Mayer, J. Alloys Compd. 491 (2010) 722–728.
[19] J.J. Jow, S.W. Yang, H.R. Chen, M.S. Wu, T.R. Ling, T.Y. Wei, Int. J. Hydrogen Energy 34 (2009) 665–671.
[20] C. Arbizzani, S. Beninati, E. Manferrari, F. Soavi, M. Mastragostino, J. Power Sources 172 (2007) 578–586.
[21] T.S. Mkwizu, M.K. Mathe, I. Cukrowski, Langmuir 26 (2010) 570–580.
[22] G.M. de Oliveira, I.A. Carlos, Electrochim. Acta 54 (2009) 2155–2163.
[23] R. Juškénas, I. Valsiuñas, V. Pakštas, R. Giraitis, Electrochim. Acta 54 (2009) 2616–2620.
[24] A.C. Sonavane, A.I. Inamdar, P.S. Shinde, H.P. Deshmukh, R.S. Patil, P.S. Patil, J. Alloys Compd. 489 (2010) 667–673.
[25] T. Matsumoto, T. Komatsu, H. Nakano, K. Arai, Y. Nagashima, E. Yoo, T. Yamazaki, M. Kijima, H. Shimizu, Y. Takasawa, J. Nakamura, Catal. Today 90 (2004) 277–281.
[26] C. Bock, C. Paquet, M. Couillard, G.A. Botton, B.R. MacDougall, J. Am. Chem. Soc. 126 (2004) 8028–8037.
[27] J.M. Sieben, M.M.E. Duarte, C.E. Mayer, ChemCatChem 2 (2010) 182–189.
[28] C.L. Green, A. Kucernak, J. Phys. Chem. B 106 (2002) 1036–1047.
[29] J.M. Sieben, M.M.E. Duarte, C.E. Mayer, J. Appl. Electrochem. 38 (2008) 483–490.
[30] J.F. Rivadulla, M.C. Vergara, M.C. Blanco, M.A. López-Quintela, J. Rivas, J. Phys. Chem. B 101 (1997) 8997–9004.
[31] W.A. Spieker, J. Liu, J.T. Miller, A.J. Kropf, J.R. Regalbuto, Appl. Catal. A 232 (2002) 219–235.
[32] V.I. Pârvulescu, S. Coman, P. Palade, D. Macovei, C.M. Teodorescu, G. Filoti, R. Molina, G. Poncelet, F.E. Wagner, Appl. Surf. Sci. 141 (1999) 164–176.
[33] M.-C. Tsai, T.-K. Yeh, C.-H. Tsai, Electrochem. Commun. 8 (2006) 1445–1462.
[34] G.A. Lawrance, Introduction to Coordination Chemistry, Wiley & Sons Inc., Great Britain, 2010.
[35] M.M.E. Duarte, A.S. Pilla, J.M. Sieben, C.E. Mayer, Electrochem. Commun. 8 (2006) 159–164.
[36] H.M. Yasin, G. Denuault, D. Pletcher, J. Electroanal. Chem. 633 (2009) 327–332.
[37] A.N. Gavrilov, O.A. Petrii, A.A. Mukovnin, N.V. Smirnova, T.V. Levtchenko, G.A. Tsirlina, Electrochim. Acta 52 (2007) 2775–2784.
[38] H. Zhang, Y. Liu, J. Zhang, C. Wang, M. Li, B. Yang, J. Phys. Chem. C 112 (2008) 1885–1889.
[39] C. Coutanceau, A.F. Rakotondrainibé, A. Lima, E. Garnier, S. Pronier, J.-M. Léger, C. Lamy, J. Appl. Electrochem. 34 (2004) 61–66.
[40] H.A. Gasteiger, N. Marković, P.N. Ross Jr., E.J. Cairns, J. Phys. Chem. 97 (1993) 12020–12029.
[41] T. Frelink, W. Visscher, J.A.R. van Veen, Langmuir 12 (1996) 3702–3708.
[44] F. Gloaguen, J.-M. Léger, C. Lamy, A. Marmann, U. Stimming, R. Vogel, Electrochim. Acta 44 (1999) 1805–1816.
[45] J.V. Zoval, J. Lee, S. Gorer, R.M. Penner, J. Phys. Chem. B 102 (1998) 1166–1175.
[46] H.-S. Oh, J.-G. Oh, Y.-G. Hong, H. Kim, Electrochim. Acta 52 (2007) 7278–7285.
[47] H. Wang, Y. Zhao, Z. Jusys, R.J. Bhem, J. Power Sources 155 (2006) 33–46.
[48] H. Wang, Z. Jusys, R.J. Behm, J. Power Sources 154 (2006) 351–359.
[49] H. Natter, R. Hempelmann, J. Phys. Chem. 100 (1996) 19525–19532.
[50] M. Watanabe, S. Motoo, J. Electroanal. Chem. 69 (1976) 429–431.
[51] R. Parsons, T. VanderNoot, J. Electroanal. Chem. 257 (1988) 9–45.
[52] A.A. Mikhaylova, O.A. Khazova, V.S. Bagotzky, J. Electroanal. Chem. 480 (2000) 225–232.
[53] A.L. Santos, D. Profeti, P. Olivi, Electrochim. Acta 50 (2005) 2615–2621.
[54] Y.E. Seidel, A. Schneider, Z. Jusys, B. Wickman, B. Kasemo, R.J. Behm, Langmuir 26 (2010) 3569–3578.
[55] Y. Zhao, X. Yang, J. Tian, Electrochim. Acta 54 (2009) 7114–7120.
[56] M.-S. Kim, B. Fang, N.K. Chaudhari, M. Song, T.-S. Bae, J.-S. Yu, Electrochim. Acta 55 (2010) 4543–4550.
[57] R. Chetty, W. Xia, S. Kundu, M. Bron, T. Reinecke, W. Schuhmann, M. Muhler, Langmuir 25 (2009) 3853–3860.
[58] S. Wang, X. Wang, S.P. Jiang, Langmuir 24 (2008) 10505–10512.
[59] X. Li, I.-M. Hsing, Electrochim. Acta 52 (2006) 1358–1365.
[60] E.R. Savinova, F. Hahn, N. Alonso-Vante, Surf. Sci. 603 (2009) 1892–1899.
[61] H.E. Hoster, A. Bergbreiter, P.M. Erne, T. Hager, H. Rauscher, R.J. Behm, Phys. Chem. Chem. Phys. 10 (2008) 3812–3823.
[62] X.E. Verykios, in: A. Wieckowski, et al. (Eds.), Catalysis and Electrocatalysis at Nanoparticle Surface, Marcel Dekker, New York, 2003 (Chapter 20).